

# Well-log analysis of pore pressure mechanisms near a minibasin-bounding growth fault at South Eugene Island field, offshore Louisiana

Matthew M. Haney<sup>1\*</sup>, Ronny Hofmann<sup>2</sup>, and Roel Snieder<sup>1</sup>

<sup>1</sup>Center for Wave Phenomena, Department of Geophysics, Colorado School of Mines, Golden, CO 80401

<sup>2</sup>Center for Rock Abuse, Department of Geophysics, Colorado School of Mines, Golden, CO 80401

\*now at: Sandia National Laboratories, Geophysical Technology Department, Albuquerque, NM 87185

## Summary

Using well log data from the South Eugene Island field, offshore Louisiana, we derive empirical relationships between elastic parameters (e.g.,  $P$ -wave velocity, density) and effective stress along both normal compaction and unloading paths. These empirical relationships provide a physical basis for numerical modeling and allow us to investigate the effect of fluid pressure. The presence of more than one stress path complicates the prediction of fluid pressure from seismically derived interval velocities since the relationship between seismic velocity and pore pressure is multi-valued.

## Introduction

Empirical relationships between pore pressure and three basic rock properties - porosity, density, and sonic velocity - are necessary for numerical modeling of the interaction of fluids and seismic wave propagation. The fact that pore pressure largely controls rock matrix properties in compacting sedimentary basins allows methods for imaging seismic reflections to indirectly measure spatially varying pore pressure distributions. In order to facilitate physically meaningful numerical modeling of fault-plane reflections arising from fluid pressure distributions, we have examined well logs for indications of pore pressure in excess of hydrostatic, or overpressures. The data for this analysis come from wells drilled at the South Eugene Island field, offshore Louisiana. The variation of the three rock properties with effective stress reveals a hysteretic behavior that occurs during the compaction of sediments. Evidence for both plastic (irreversible) and elastic (reversible) deformation exists in the available well data and pressure tests. These two regimes point to different underlying causes of overpressure (Hart, 1995). For these dual deformation mechanisms, we construct two empirical relationships between each rock property and pore pressure - one valid for each regime.

## Porosity versus depth

Compaction acts to reduce the porosity of sediments as they are buried; however, this process can continue only as long as fluids in the diminishing pore space are allowed to be expelled. Such would be the case in normally

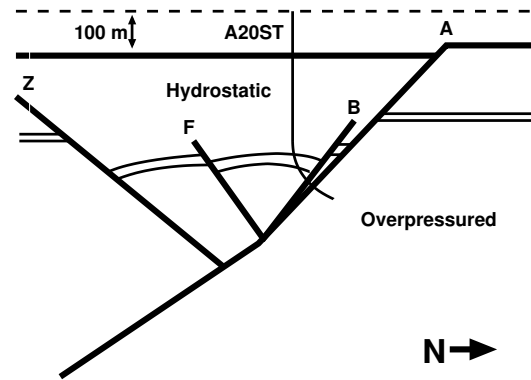


Fig. 1: Cartoon depth section (bottom) of the subsurface at South Eugene Island. The four main growth faults are shown in the bottom panel as the A, B, F, and Z faults. Throw across the faults is depicted by the layer running from left to right. Most of the wells at South Eugene Island were drilled into the shallow, hydrostatic section; the A20ST well was unusual in that it was continued through the A-fault system and into the deep overpressured compartment.

pressured, hydrostatic sediments in which the fluids are in communication up to the seafloor. Once the movement of the fluids out of the pore space is opposed, as in a compartment sealed-off by low permeability or high capillary-entry-pressure shales or fault gouge, the porosity remains constant with burial depth if the fluid is more or less incompressible. This situation is called *undercompaction* (Huffman, 2002). Undercompaction means the sediments are “frozen” in time and are simply buried in their unchanging earlier compaction state (Bowers, 1995). To compound the situation, if fluid from outside the undercompacted sediments is pumped into the pore space, or if hydrocarbons are generated from within the undercompacted sediments, a process called *unloading* occurs. Whereas undercompaction can only cease the reduction of porosity, unloading can actually reverse the trend and increase porosity. Although unloading can reverse the trend, it cannot reclaim all of the previously lost porosity. This is because the compaction process has a large *irreversible* component. In contrast, unloading and loading of sediments by pumping fluid into and then depressurizing the pore space is a reversible process, insofar as the fluid does not cause hydrofracturing.

We have studied wireline data taken in wells at the South Eugene Island field, offshore Louisiana, for indicators of overpressure, such as constant porosity as a function of

## Overpressure mechanisms near a fault

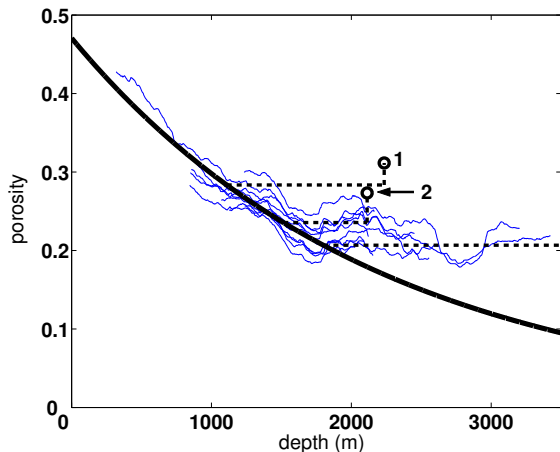


Fig. 2: Porosity versus depth at South Eugene Island. The thick, solid line is the best-fit normal compaction trend using Athy's Law. The faint solid lines are density-derived porosity values from 11 wells at South Eugene Island. To obtain the porosity, we assume that the solid grains have a density of  $2650 \text{ kg/m}^3$  and the fluid has a density of  $1000 \text{ kg/m}^3$ , as in Revil and Cathles (2002). There is a clear break from the shallow, exponentially decreasing porosity trend at a depth of 1800 m, at which point the porosity remains constant with increasing depth, as shown by the flat dashed line. The two circles are density-derived porosities from the upthrown block to the north of the minibasin at South Eugene Island. The dashed lines connecting the circles to the main compaction trend are the interpreted porosity histories of the samples. They show a period of undercompaction, depicted as a horizontal line deviating from the normal compaction trend, followed by a vertical unloading path due to a late-stage pore-pressure increase.

depth. Previous work by Hart *et al.* (1995) shows the crossover from hydrostatic to overpressured conditions in porosities derived from sonic velocities. Here, we take a slightly different, perhaps more straightforward approach based on the density log. The South Eugene Island field is a Plio-Pleistocene minibasin formed by salt withdrawal and has yielded more than 300 million barrels of oil in its lifetime. A cartoon depiction of the subsurface at South Eugene Island is displayed in Fig. 1. The main part of the field is a vertical stack of interbedded sand and shale layers bounded by two large growth faults to the north and south.

Fig. 2 shows porosity derived from density logs taken in the following wells at South Eugene Island: A13, A20ST, A14OH, A15, A23, A6, B10, B1, B2, B7, and B8. Because the geology in the minibasin is essentially horizontally layered, we ignore the fact that some wells may be miles away from each other and simply look at the depth variation of their porosity. In all the well logs shown in this paper, we have done some smoothing with depth (over  $\sim 100 \text{ m}$ ) to remove any short-range lithologic influences (e.g., sand versus shale) on the density and velocity. To obtain the porosity from the density log, we take the solid grains to have a density of  $2650 \text{ kg/m}^3$  and the fluid to have a density of  $1000 \text{ kg/m}^3$ , as in Revil and Cathles (2002). There is a clear break from the shallow, decreasing poros-

ity trend at a depth of 1800 m. We take this depth as the onset of overpressures in the sedimentary section, beneath a shale bed located above a layer called the JD-sand. By fitting an exponential trend to the porosity values above 1800 m, we get the normal compaction trend in the hydrostatically pressured sediments

$$\phi^c(z) = 0.47 e^{-0.00046 z}, \quad (1)$$

where, in this equation, the depth  $z$  is in meters. The superscript  $c$  in equation (1) refers to the fact that this functional relationship characterizes normal compaction. In the porosity-versus-depth plot of Fig. 2, this relationship holds for any movement toward the right on the normal compaction curve and any purely right-going horizontal deviations from the normal compaction curve. For purely right-going horizontal deviations, the depth  $z$  used in equation (1) is equal to the depth at which the horizontal deviation started. The two circles in Fig. 2, represent samples taken in the A20ST well and are connected to the normal compaction curve by both horizontal and vertical lines. The vertical lines show the departure of the samples from the normal compaction trend. We return to these in the next section. Note that the sediments deeper than 1800 m in Fig. 2 maintain a nearly constant porosity of around 0.2 during subsequent burial (a horizontal deviation from the compaction trend).

## Density versus vertical effective stress

Since bulk density, and not porosity, is a more widely used parameter in simulations of seismic wave propagation, we have studied the variation of bulk density with fluid pressure. By looking at bulk density, we also leave the original data, a density log, unaltered by assuming certain solid and fluid densities. In contrast to the preceding section, we want to see how density changes with effective stress, instead of depth. To accomplish this, we take only the measurements that are shallower than 1800 m, where the pore pressure is, by all indications, hydrostatic. Therefore we know the pore pressure and can calculate the effective stress. In overpressured compartments, since the pore pressure is unknown, direct measurements by Repeat Formation Tests (RFTs) are necessary to calculate the effective stress.

We rewrite equation (1) in terms of density and effective stress using the relationships

$$\rho = \rho_s(1 - \phi) + \phi\rho_f, \quad (2)$$

and

$$\sigma_d = \rho_f g z, \quad (3)$$

where  $\rho$  is the bulk density and  $\rho_s$  and  $\rho_f$  are the densities of the solid and fluid components. Note that the relationship for  $\sigma_d$  holds only under hydrostatic conditions. From these relationships and equation (1), we obtain the normal compaction curve for density

$$\rho^c(\sigma_d) = \rho_s - 0.47(\rho_s - \rho_f) e^{-0.0003\sigma_d}, \quad (4)$$

## Overpressure mechanisms near a fault

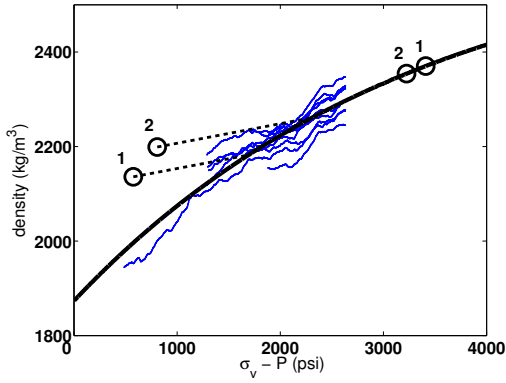


Fig. 3: Density versus effective stress at South Eugene Island. The thick solid line is the same normal compaction trend shown in Fig. 2, except transformed into density and effective stress. The faint solid lines are also the same as in Fig. 2, except that they are now limited to the hydrostatic depths down to 1800 m. The circles represent two pressure measurements, labeled 1 and 2, which were made in the overpressured upthrown block where a density log also existed. For each pressure measurement, we plot the data point twice - one where it should lie on the normal compaction curve were it to have been normally pressured, and the other where it actually does plot because of severe overpressure. Note that sample 1 is from a greater depth than sample 2.

where  $\rho_s$  and  $\rho_f$  are the densities of the solid and fluid components, taken as  $2650 \text{ kg/m}^3$  and  $1000 \text{ kg/m}^3$  respectively, and  $\sigma_d$  is in psi. We plot this normal compaction curve in Fig. 3 together with the density measurements. Also, in Fig. 3, we show as circles two data points obtained from RFT pressure measurements and density log measurements in the overpressured upthrown block. We show the circles in two locations - one on the normal compaction trend where they would plot if the measurements were at hydrostatically pressured locations, and the other where they actually plot because of severe overpressures being present in the upthrown block.

At this point, we don't know exactly how the samples taken in the upthrown block came to be off the normal compaction trend. Using a laboratory measurement of the unloading coefficient by Elliott (1999) on a core sample taken near the locations of samples 1 and 2, the path that these samples took to their present locations can be estimated. Elliott (1999) characterized the unloading, or elastic swelling, for the porosity of the core samples to be

$$\phi^u(\sigma_d) = \phi_0 (1 - \beta \sigma_d), \quad (5)$$

where  $\phi_0$  and  $\beta$  characterize the deviation of the unloading path from the normal compaction trend. Note the superscript  $u$ , in contrast to equation (1), indicating the unloading path instead of the normal compaction trend. Elliott (1999) found that  $\phi_0 = 0.37$  and  $\beta = 0.98 \times 10^{-8} \text{ Pa}^{-1}$  for the unloading path. Though these parameters describe the porosity, we use them to find the slope of the unloading path for density using the relationships between porosity and density described earlier. After finding this slope, we can construct the unloading path for

the density from equation (4) and the slope

$$\rho^u(\sigma_d) = 0.04 (\sigma_d - \sigma_{max}) + \rho_s - 0.47 (\rho_s - \rho_f) e^{-0.0003\sigma_{max}}. \quad (6)$$

This expression contains an extra parameter  $\sigma_{max}$  that refers to the value of the effective stress when the sample began to be unloaded. We do not know  $\sigma_{max}$  for samples 1 and 2, but we do know that  $\sigma_{max}$  must lie on the main compaction trend. Hence, we can construct linear unloading paths for the density, as shown by the dashed lines in Figure 3. With these unloading paths, we can then find the value for the maximum past effective stress  $\sigma_{max}$ . It is worth mentioning that the maximum past effective stress for sample 1 comes out to be  $\sim 1500$  psi by our approach of using Elliott's experimental results. In an independent measurement, Stump and Flemings (2002) performed uniaxial strain tests on a core sample taken from the same location as sample 1 to find the maximum past effective stress. Stump and Flemings (2002) report a value of 1248 psi for this sample, close to our estimate of  $\sim 1500$  psi; visually, the discrepancy lies within the error bars of the normal compaction curve's fit to the density log data.

With the estimate of the maximum past effective stress, we can also return to Fig. 2 and find the depth at which samples 1 and 2 left the normal compaction trend, since in the hydrostatic zone the depth is a linearly scaled version of the effective stress. These depths correspond to a slightly lower porosity than that of samples 1 and 2. We interpret this as being the result of a late stage porosity increase and represent it as a vertical unloading path for samples 1 and 2 in Fig. 2.

## Sonic velocity versus vertical effective stress

For the purposes of modeling faults and to make inferences about the distribution of pore pressure from seismic interval velocity inversions, accurate pore-pressure-versus-velocity relationships are critical. In general, sonic velocity has a normal compaction curve and unloading paths as a function of effective stress that are similar to those we just described for the density well log data. To obtain these relationships, we proceed as for the density logs: 1) We take 12 shallow wells to make up a data set of sonic velocity versus effective stress. 2) We select the depth range with hydrostatic pressures and plot the sonic velocity versus effective stress. 3) We fit this with a power law relation for the normal compaction trend. 4) We then look at where the two samples from the overpressured upthrown block lie and construct unloading curves using the estimate for the maximum past effective stress that we obtained in the previous section on density. The wells we use for characterizing the sonic velocity come from A20ST, A14OH, A23, A6, B10, B1, B2, B7, B8, A1, B14, and B20.

In Fig. 4, we plot the normal compaction trend for sonic velocity as a thick solid line described by the power law

## Overpressure mechanisms near a fault

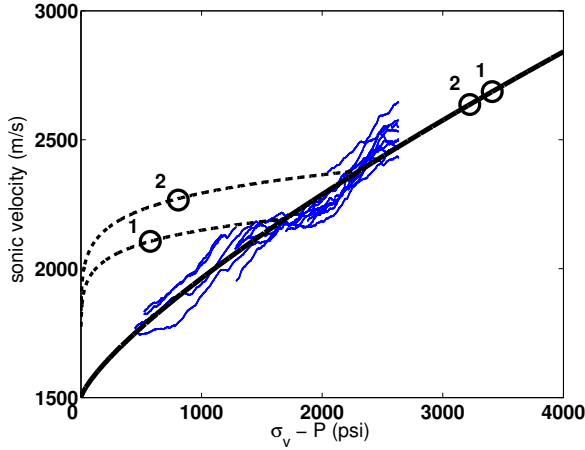


Fig. 4: Sonic velocity versus effective stress at South Eugene Island. The thick solid line represents the normal compaction curve fitted to the shallow well data, shown in the faint solid lines. We also plot samples 1 and 2 both where they should fall on the normal compaction trend, were they to be normally pressured, and where they actually plot due to the severe overpressure where they were obtained. Using the estimate for past maximum effective stress from the density plot and the Bowers-type relation (Bowers, 1995) shown in equation (8), we are able to construct the velocity unloading curves, shown as dashed lines.

equation (Bowers, 1995)

$$v_p^c(\sigma_d) = 1500 + 2.3 \sigma_d^{0.77}, \quad (7)$$

where the  $P$ -velocity is in m/s and differential pressure is in psi. Note again the superscript for the normal compaction relation. We also construct the unloading curve for  $v_p$  following the relationship first suggested by Bowers (1995)

$$v_p^u(\sigma_d) = 1500 + 2.3 \left[ \sigma_{max} \left( \frac{\sigma_d}{\sigma_{max}} \right)^{1/6.2} \right]^{0.77}, \quad (8)$$

where  $\sigma_d$  and  $\sigma_{max}$  are in psi and  $v_p$  is again in m/s.

To model elastic waves, one other parameter is needed in addition to  $\rho$  and  $v_p$ ; for instance, a seismologist would naturally want the shear velocity. In the absence of information on the shear wave velocity  $v_s$  and pressure in the shallow, hydrostatic sediments, we assume that

$$v_s(\sigma_d) = v_p(\sigma_d) - 1500, \quad (9)$$

where this relationship holds on both the normal compaction curve and the unloading path. The data presented by Zimmer *et al.* (2002) for unconsolidated sands supports this assumption, in that the dependence they found for  $v_s$  on effective stress is essentially a down-shifted version of the  $v_p$  curve. An additional piece of supporting evidence comes from the only  $v_s$  data available at South Eugene Island, a shear log from the A20ST well, where samples 1 and 2 were taken. There, the ratio of  $v_p/v_s$  from the sonic and shear logs falls between 3 to 3.5 in the overpressured upthrown block.

## Conclusion

We have established two empirical relationships between each of three basic rock properties and pore pressure at the South Eugene Island field. Most important for subsequent numerical modeling of seismic wave propagation, we have found relationships for the density  $\rho$  and the sonic velocity  $v_p$  on both the normal compaction and unloading paths. We plan to use the empirical relationships between the elastic parameters and fluid pressure to simulate fault-plane reflections from different pressure distributions around fault zones.

## Acknowledgments

We thank Shell International Exploration and Production for access to the well log data and to Jon Sheiman for helpful discussions on pore pressure.

## References

- Bowers, G. L., 1995, Pore Pressure Estimation from Velocity Data: Accounting for Overpressure Mechanisms Besides Undercompaction: SPE Drilling & Completion, **June**, 89-95.
- Elliott, D. A., 1999, *Hydrofracture Permeability Response and Maximum Previous Consolidation Stress Estimations for Faulted and Micro-Faulted Silty-Shales Taken from the Eugene Island Block 330 Field Pathfinder Well in the Gulf of Mexico*. MSc Thesis, University of California, San Diego.
- Hart, B. S., Flemings, P. B., and Deshpande, A., 1995, Porosity and pressure: Role of compaction disequilibrium in the development of geopressures in a Gulf Coast Pleistocene basin: *Geology*, **23**, 45-48.
- Huffman, A. R., 2002, The future of pore-pressure prediction using geophysical methods: *The Leading Edge*, **21**, 199.
- Revil, A. and Cathles III, L. M., 2002, Fluid transport by solitary waves along growing faults: A field example from the South Eugene Island Basin, Gulf of Mexico: *Earth and Planetary Science Letters*, **202**, 321-335.
- Stump, B. B. and Flemings, P. B., 2002, Consolidation State, Permeability, and Stress Ratio as Determined from Uniaxial Strain Experiments on Mudstone Samples from the Eugene Island 330 Area, Offshore Louisiana in: *Pressure regimes in sedimentary basins and their prediction*, eds. A. Huffman and G. Bowers, AAPG Memoir 76.
- Zimmer, M., Prasad, M., and Mavko, G., 2002, Pressure and porosity influences on  $V_P - V_S$  ratio in unconsolidated sands: *The Leading Edge*, **21**, 178-183.